A higher order perfectly matched layer formulation for finite-difference time-domain seismic wave modeling

A Higher-Order correction PML to increase FDTD seismic wave absorption

ABSTRACT

A higher order Perfectly Matched Layer (PML) formulation is presented to improve the absorption performance for finite difference time domain seismic modelling. Firstly a new unsplit 'correction' approach is outlined, which allows for traditional, first order PML's to be added directly to existing codes in a straightforward manner. Then, using this framework, a PML formulation is developed that can be used to construct higher order PML's of arbitrary order. The greater number of degrees of freedom associated with the higher order PML allows for enhanced flexibility of the PML stretching functions, thus potentially facilitating enhanced absorption performance. It is found that the new approach can offer increased elastodynamic absorption, particularly for evanescent waves. It is also discovered that the extra degrees of freedom associated with the higher order PML require careful optimisation if enhanced absorption is to be achieved. Furthermore, these extra degrees of freedom increase the computational requirements in comparison to first order schemes. The formulations are presented using one compact equation thus increasing the ease of implementation. Additionally, the formulations are based on a recursive integration approach which reduces PML memory requirements, and do not require special consideration for corner regions. The new formulations are tested to determine their ability to absorb body waves and surface waves. Both standard staggered grid stencils, and rotated staggered grid stencils are also tested.

INTRODUCTION

Finite difference time domain (FDTD) modelling techniques are commonly used to simulate elastodynamic wave propagation for the purposes of seismic exploration. Absorbing boundary conditions (ABC's) are typically placed at domain edges to prevent boundary reflections contaminating results. The ABCs performance dictates how far it can be placed from the modelling areas of concern without causing reflections. Therefore a highly effective ABC can be placed in close proximity to the modelling area of interest, thus significantly reducing the computational workload.

Damping zones (Cerjan et al., 1985), continued fraction conditions(Guddati and Lim, 2006), optimised boundary conditions (Peng and Toksoz, 1995), viscous boundaries (Lysmer and Kuhlemeyer, 1969), (Kouroussis et al., 2011), paraxial conditions (Higdon, 1986) and non-local operators (Hagstrom and Hariharan, 1998) approaches have been

attempted to absorb outgoing seismic waves. Although these techniques generally performed well for waves arriving perpendicular to the boundary, their performance was reduced for waves impinging at low angles of incidence. This is undesirable for 2D/3D seismic wave modelling because the wave patterns are composed of large variations in incident angle.

(Berenger, 1996), (Berenger, 1994) introduced a 'Perfectly matched layer' (PML) technique to absorb electromagnetic waves (i.e. Maxwell's equations) using a series of finite layers, each with identical material properties to the modelling domain, to gradually damp outgoing waves. It offered high performance and was capable of absorbing waves independent of arrival angle. (Chew and Weedon, 1994) quickly extended this PML formulation to include a stretching of both real and imaginary spatial co-ordinates, thus offering the potential for additional absorption.

Using a similar implementation to the electromagnetic wave approach, (Chew and Lui, 1996) adapted the PML condition to offer absorption for seismic waves. Since then, several approaches have been used to implement PML conditions for elastodynamic problems (Hastings et al., 1996), (Basu and Chopra, 2004), (Basu, 2009). One drawback of such approaches was that reflections were encountered at large grazing incidences. This was because although the PML reflection coefficient was theoretically zero before discretisation, after discretisation it was not zero. Analytical expressions were used to overcome this for the electromagnetic case however due to the increased complexity of the underlying elastodynamic equations, this was more challenging (Collino and Tsogka, 2001).

An alternative approach for electromagnetics was to modify the complex coordinate stretching function within the PML (Roden and Gedney, 2000),(Kuzuoglu and Mittra, 1996). This C-PML or CFS-PML (complex frequency shifted) was a more attractive option for the elastodynamics case and therefore was further explored by (Festa and Vilotte, 2005). The theory behind this method was that it would offer much improved absorption for waves propagating at low grazing angles (i.e. for long distances within the PML region). The CFS-PML proved popular and has since been developed for poroelastic (Martin et al., 2008) and anisotropic media (Becache et al., 2003).

Early CFS-PML conditions were implemented using an artificial splitting of velocity and stress fields, in a similar manner to some of the early non CFS-PML conditions including (Chew and Weedon, 1994). This splitting procedure made PML implementation in traditional FDTD codes challenging because two different sets of equations were required for each PML and non-PML region. In addition, such implementations were not well-posed mathematically (Abarbanel and Gottlieb, 1997).

To avoid field splitting, convolution terms (Komatitsch and Martin, 2007), auxiliary differential equations (Martin et al., 2010) and integration approaches (F. H. Drossaert and

Giannopoulos, 2007) were also investigated. As convolution is generally regarded as computationally inefficient, recent focus has shifted to auxiliary differential equation (ADE) and integral term implementations.

(Martin et al., 2010) outlined a non-convolutional ADE PML approach where a fourth-order Runge-Kutta scheme was used in conjunction with eighth order Holberg space discretization. This formulation was shown to have high accuracy and to be stable for up to 100,000 timesteps. Additionally, (Martin et al., 2010) investigated the potential to extend this ADE-PML condition to higher order PML's but concluded that no significant performance benefit was capable.

(Zhang and Shen, 2010) built on the work of (Martin et al., 2010) and outlined a similar ADE-PML fourth-order Runge-Kutta scheme that resulted in a complete set of first order differential equations. This meant that the same FDTD implementation could be used to solve both the ADE C-PML equations and the interior domain equations.

An alternative approach to avoid field splitting was outlined by (F. H. Drossaert and Giannopoulos, 2007) through the use of recursive integration (RI-PML). This technique used an extended trapezoidal rule to integrate the PML time derivatives thus negating the requirement to split fields or use an ADE formulation. The RI-PML approach required an equal amount of memory in comparison to split-field formulations and slightly less memory than the ADE approach.

One of the shortcomings of using the new complex frequency shifted PML was that although it offered improved absorption for low incident waves, the application of the underlying filter reduced the absorption performance of the PML for waves arriving at high incidences (i.e. at 90 degree angles).

In an attempt to maximise absorption for both low and high incidence waves for electromagnetic wave modelling, (Correia and Jin, 2005) proposed higher order PML formulations. These formulations used a combination of non-CFS and CFS stretching functions. It was found that enhanced performance was achievable because the non-CFS component aided in the absorption of high incident waves whereas the CFS component aided the absorption of the low incident waves.

This paper extends the PML implementation described by (Giannopoulos, 2011) to the seismic wave equation using a RI-PML approach. It does so based on a new and improved 'correction PML' implementation approach, which is also outlined. The higher order PML has the potential to utilise a greater number of degrees of freedom in comparison to the traditional first order PML condition, thus offering greater absorption. Improved absorption is desirable because it allows for reduced domain sizes, which is particularly important for 3D problems (Kouroussis et al., 2014), (Laghrouche and Le

Houédec, 1994). This potential for increased absorption is highlighted through several comparisons with alternative first order PML conditions. It should be noted that although the new PML is termed 'higher order', this has no bearing on its compatibility with space and time discretisation.

IMPLEMENTING PML THROUGH A CORRECTION TECHNIQUE

To derive the new time domain correction PML, it was first necessary to work in the frequency domain before transferring back to the time domain and then using the trapezoidal rule to solve the resulting integral. Therefore, using a stretched coordinate system, the two-dimensional frequency domain elastodynamic velocity-stress equations (based on the original time domain equations as outlined by (Virieux, 1986) and (Graves, 1996)) took the form:

$$j\omega\tilde{v}_x = b\left(\frac{1}{s_x}\frac{\partial\tilde{\sigma}_{xx}}{\partial x} + \frac{1}{s_z}\frac{\partial\tilde{\sigma}_{xz}}{\partial z}\right) \tag{1}$$

$$j\omega\tilde{v}_z = b\left(\frac{1}{s_x}\frac{\partial\tilde{\sigma}_{xz}}{\partial x} + \frac{1}{s_z}\frac{\partial\tilde{\sigma}_{zz}}{\partial z}\right) \tag{2}$$

$$j\omega\tilde{\sigma}_{xx} = (\lambda + 2\mu)\frac{1}{s_x}\frac{\partial\tilde{v}_x}{\partial x} + \lambda\frac{1}{s_z}\frac{\partial\tilde{v}_z}{\partial z} \tag{3}$$

$$j\omega\tilde{\sigma}_{zz} = (\lambda + 2\mu)\frac{1}{s_z}\frac{\partial\tilde{v}_z}{\partial z} + \lambda\frac{1}{s_x}\frac{\partial\tilde{v}_x}{\partial x} \tag{4}$$

$$j\omega\tilde{\sigma}_{xz} = \mu\left(\frac{1}{s_x}\frac{\partial\tilde{v}_z}{\partial x} + \frac{1}{s_z}\frac{\partial\tilde{v}_x}{\partial z}\right) \tag{5}$$

Where the frequency domain velocity and stress components were denoted by $\tilde{v}$ and $\tilde{\sigma}$ respectively, and ω representing circular frequency. λ and μ were the lames coefficients and b was buoyancy. The co-ordinate axis were defined by x and z, and s_x and s_z were the PML stretching functions (in the x and z directions respectively), which served to absorb outgoing waves.

$$s_{u_i} = \kappa_{u_i} + \frac{d_{u_i}}{\alpha_{u_i} + j\omega} \tag{6}$$

d_{u_i}, κ_{u_i} and α_{u_i} were the attenuation coefficients used to describe the loss within the PML region. The subscript u was used to denote the staggered grid component, e.g. stress/velocity, and the subscript i was used to describe the direction of attenuation ($u \in [u, v]$ and $i \in [x, z]$). Additionally, the variable transform $j = \sqrt{-1}$, and ψ_u were defined as

$$\psi_u = \frac{1 - s_u}{s_u} = \frac{1}{s_u}\left(\frac{1 - s_u}{1}\right) = \frac{1}{s_u} - 1 \tag{7}$$

Or

$$\frac{1}{s_u} = (1 + \psi_u) \tag{8}$$

Rearranging equations 1-5. in terms of ψ_u gave

$$j\omega\tilde{v}_x = b\left((1 + \psi_x)\frac{\partial\tilde{\sigma}_{xx}}{\partial x} + (1 + \psi_z)\frac{\partial\tilde{\sigma}_{xz}}{\partial z}\right) \tag{9}$$

$$j\omega\tilde{v}_z = b\left((1 + \psi_x)\frac{\partial\tilde{\sigma}_{xz}}{\partial x} + (1 + \psi_z)\frac{\partial\tilde{\sigma}_{zz}}{\partial z}\right) \tag{10}$$

$$j\omega\tilde{\sigma}_{xx} = (\lambda + 2\mu)(1 + \psi_x)\frac{\partial\tilde{v}_x}{\partial x} + \lambda(1 + \psi_z)\frac{\partial\tilde{v}_z}{\partial z} \tag{11}$$

$$j\omega\tilde{\sigma}_{zz} = (\lambda + 2\mu)(1 + \psi_z)\frac{\partial\tilde{v}_z}{\partial z} + \lambda(1 + \psi_x)\frac{\partial\tilde{v}_x}{\partial x} \tag{12}$$

$$j\omega\tilde{\sigma}_{xz} = \mu\left((1 + \psi_x)\frac{\partial\tilde{v}_z}{\partial x} + (1 + \psi_z)\frac{\partial\tilde{v}_x}{\partial z}\right) \tag{13}$$

A comparison between equations 1-5 and 9-13 revealed that the stretched velocity/stress equations were analogous to an addition of field dependant variables. To display this with greater clarity, equations 9-13 were rearranged and rewritten as:

$$j\omega\tilde{v}_x = b\left(\frac{\partial\tilde{\sigma}_{xx}}{\partial x} + \frac{\partial\tilde{\sigma}_{xz}}{\partial z}\right) + b(\tilde{J}_{xx} + \tilde{J}_{xz}) \tag{14}$$

$$j\omega\tilde{v}_z = \tilde{b}\left(\frac{\partial\tilde{\sigma}_{xz}}{\partial x} + \frac{\partial\tilde{\sigma}_{zz}}{\partial z}\right) + b(\tilde{J}_{xz} + \tilde{J}_{zz}) \tag{15}$$

$$j\omega\tilde{\sigma}_{xx} = (\lambda + 2\mu)\frac{\partial\tilde{v}_x}{\partial x} + \lambda\frac{\partial\tilde{v}_z}{\partial z} + \left((\lambda + 2\mu)\tilde{M}_{xx} + \lambda\tilde{M}_{xz}\right) \tag{16}$$

$$j\omega\tilde{\sigma}_{zz} = (\lambda + 2\mu)\frac{\partial\tilde{v}_z}{\partial z} + \lambda\frac{\partial\tilde{v}_x}{\partial x} + \left((\lambda + 2\mu)\tilde{M}_{zz} + \lambda\tilde{M}_{zx}\right) \tag{17}$$

$$j\omega\tilde{\sigma}_{xz} = \mu\left(\frac{\partial\tilde{v}_z}{\partial x} + \frac{\partial\tilde{v}_x}{\partial z}\right) + \mu\left(\tilde{M}_{zx} + \tilde{M}_{xz}\right) \tag{18}$$

Where $\tilde{J}$ was a field dependent variable used to correct the velocity components and $\tilde{M}$ was a field dependent variable used to correct the stress components. $\tilde{J}$ and $\tilde{M}$ were given by:

$$\tilde{J}_{xu} = \psi_u \frac{\partial \tilde{\sigma}_{xu}}{\partial u} \tag{19}$$

$$\tilde{M}_{xu} = \psi_u \frac{\partial \tilde{v}_v}{\partial u} \tag{20}$$

with $u,\ v \in \{x, z\}$ and $u \neq v$.

From equations 14-18 it was clear that the velocity and stress values of the stretched coordinates in the PML region (i.e. where $\psi_u \neq 0$) could be calculated through an addition of equations 19 and 20 to the previously calculated velocity and stress values. Thus, for an existing FDTD script, the field dependent variables could be simply added to the regions where absorption was required.

To do so, first the original update equations are computed as if there is no PML present (i.e. rigid boundary condition), using arbitrary time stepping techniques such as those described in (Graves, 1996) or (Virieux, 1986). Then, the cells within the PML regions are updated by adding the correction terms to the original values as previously calculated. This can be seen as 'correcting' the original update terms to account for the presence of the PML. In comparison, for traditional non-correction PML schemes such as (Komatitsch and Martin, 2007), the stress and velocity values are calculated at the same instance for both the interior domain and the PML regions. This can impact on the ease of implementation.

Therefore, the key benefits of the new first order correction PML:

1. When adding PML to an existing code, no revisions to the original code need to be made
2. PML corner regions do not require any special consideration
3. Programming complexity is significantly reduced

It should be noted that equations 14-18 were cast in the frequency domain. To calculate the equivalent time domain equations, recursive integration is required. The following section describes this process for the development of a higher order PML, using this correction approach. Therefore, the resulting equations needed to calculate the first order time domain correction terms, are described by equations 62-66.

DEVELOPMENT OF A HIGHER ORDER PML

The new correction PML (equations 14-18) facilitated straightforward implementation of the PML stretching functions because it's formulation did not require any modification of the underlying FDTD update scheme. This made it well suited to

provide a foundation for implementing arbitrary stretching functions. Therefore it was used to provide an efficient and straightforward PML formulation for N^{th} order stretching.

Stretching Function Definitions

For the 2D case, six correction terms were required to describe the attenuation of all velocity and stress field variables (three J_{uu} for velocity terms and three M_{uu} for stress terms). Despite this, for brevity, only the derivation of J_{xz} (i.e. the correction term required to partly describe the stretching of the velocity components) is outlined. All other correction terms (J_{uu} and M_{uu}) can be found analogously.

Firstly, equation 7 and equation 19, were combined which led to,

$$\tilde{J}_{xz} = \left(\frac{1}{s_u} - 1\right)\frac{\partial \tilde{\sigma}_{xu}}{\partial u} \tag{21}$$

Then, considering only the vertical components (i.e. $u = z$) and rearranging resulted in

$$\frac{\partial \tilde{\sigma}_{xz}}{\partial z} = s_z\left(\tilde{J}_{xz} + \frac{\partial \tilde{\sigma}_{xz}}{\partial z}\right) \tag{22}$$

Additionally, for N^{th} order stretching the overall stretching function was defined as:

$$s_u = \prod_{i=1}^{N} s_{u_i} \tag{23}$$

This meant that the overall stretching function was the product of all other stretching functions from $1 - N$. When combined with equation 22 this yielded:

$$\frac{\partial \tilde{\sigma}_{xz}}{\partial z} = \left(\prod_{i=1}^{N} s_{z_i}\right)\left(\tilde{J}_{xz} + \frac{\partial \tilde{\sigma}_{xz}}{\partial z}\right) \tag{24}$$

Where $N \in [\Re]$ meaning that potentially the combination of an infinite number of stretching functions could be calculated. Despite this, it was possible to define the stretching functions needed to describe the overall stretching function, using only three sets of i.

- One stretching function for the first order stretch ($i = 1$)
- One stretching function for the final order stretch ($i = N$)
- One stretching function for all the stretching functions between the first and last ($1 < i < N$)

To calculate these three stretching functions, a set of functions Ψ_{xz_i} were defined for $i \in [1, N-1]$

$$\Psi_{xz_i} = \left(\prod_{m=i+1}^{N} s_{z_m} \right) \left(\tilde{J}_{xz} + \frac{\partial \tilde{\sigma}_{xz}}{\partial z} \right) \tag{25}$$

Using equations 24 and 25 to eliminate $\tilde{J}_{xz}$ led to

$$\frac{\partial \tilde{\sigma}_{xz}}{\partial z} / \Psi_{xz_i} = s_{z_i} \tag{26}$$

Therefore, the first order stretching function ($i = 1$) was equivalent to

$$\Psi_{xz_1} = \frac{1}{s_{z_1}} \frac{\partial \tilde{\sigma}_{xz}}{\partial z} \tag{27}$$

Then combining equations 22 and 27 allowed for the calculation of equation 28. This was used to describe the stretching function between the first and the final stretching function ($i \in [2, N-1]$)

$$\Psi_{xz_i} = \frac{1}{s_{z_i}} \Psi_{i-1} \tag{28}$$

Lastly, combining equations 22 and 28 resulted in the final stretching function ($i = N$)

$$\left(\tilde{J}_{xz} + \frac{\partial \tilde{\sigma}_{xz}}{\partial z} \right) = \frac{1}{s_{z_N}} \Psi_{xz_{N-1}} \tag{29}$$

Domain Transformation

The stretching functions 27-29 were defined using frequency domain terms. To implement them within a time domain finite difference model they had to be reformulated in the time domain.

To facilitate this transformation, firstly the stretching function 6 was substituted into 26 giving

$$\kappa_{z_1} \Psi_{xz_1} + \frac{d_{z_1}}{\alpha_{z_1} + i\omega} \Psi_{xz_1} = \frac{\partial \tilde{\sigma}_{xz}}{\partial z} \tag{30}$$

With the intention of solving for Ψ_{xz_1}, both sides were multiplied by $(\alpha_{z_1} + i\omega)$

$$(\alpha_{z_1}\kappa_{z_1} + d_{z_1})\Psi_{xz_1} + i\omega\kappa_{z_1}\Psi_{xz_1} = \alpha_{z_1}\frac{\partial\tilde{\sigma}_{xz}}{\partial z} + i\omega\frac{\partial\tilde{\sigma}_{xz}}{\partial z} \tag{31}$$

To prime equation 31 for transformation it was rearranged and similar terms were grouped together,

$$\Psi_{xz_1} = \frac{1}{\kappa_{z_1}}\frac{\partial\tilde{\sigma}_{xz}}{\partial z} + \frac{1}{i\omega}\left[\frac{\alpha_{z_1}}{\kappa_{z_1}}\frac{\partial\tilde{\sigma}_{xz}}{\partial z} - \frac{(\alpha_{z_1}\kappa_{z_1} + d_{z_1})}{\kappa_{z_1}}\Psi_{xz_1}\right] \tag{32}$$

The relationship $\frac{1}{i\omega}\tilde{A}(w) = \int_0^t A(t)\delta t$ was then used to make the transform trivial. The post-transformation stretching function was equivalent to the domain integral

$$\Psi_{xz_1} = \frac{1}{\kappa_{z_1}}\frac{\partial\sigma_{xz}}{\partial z} + \int_0^t \frac{\alpha_{z_1}}{\kappa_{z_1}}\frac{\partial\sigma_{xz}}{\partial z} - \frac{(\alpha_{z_1}\kappa_{z_1} + d_{z_1})}{\kappa_{z_1}}\Psi_{xz_1}\ \delta t \tag{33}$$

Application of the Extended Trapezoidal Rule

The time integral, (equation 32), was not yet ready to be implemented within a FDTD scheme. For PML applications, the high accuracy and low memory requirements associated with using the trapezoidal integration rule (F. H. Drossaert and Giannopoulos, 2007) have made it an attractive choice. Therefore this was the approach taken.

The higher order PML can be implemented in any staggered grid FDTD formulation, of arbitrary order. For the purpose of this derivation, it's implementation was assumed to be within a velocity-stress grid with first order accuracy that was staggered in both space and time. Therefore, if 't' was time, when t = n the velocity components were first calculated and then the PML regions were updated.

It should be noted that all field quantities were assumed to be zero for $t \leq 0$. Also, the index notation J_{a1}^{a2}, was utilised, where $a1$ defined the index for spatial discretization and $a2$ denoted the index for time discretization. Consequently, the application of the extended trapezoidal rule resulted in:

$$\Psi_{xz_1}^{n+\frac{1}{2}} = \frac{1}{\kappa_{z_1}}\frac{\partial\sigma_{xz}^{n+\frac{1}{2}}}{\partial \mathrm{z}} + \tag{34}$$

$$\sum_{p=0}^{n-1}\left[\frac{\alpha_{z_1}\Delta t}{\kappa_{z_1}}\frac{\partial\sigma_{xz}^{p+\frac{1}{2}}}{\partial z}-\frac{(\alpha_{z_1}\kappa_{z_1}+d_{z_1})\Delta t}{\kappa_{z_1}}\Psi_{xz_1}^{p+\frac{1}{2}}\right]$$
$$+\frac{\Delta t}{2}\frac{\alpha_{z_1}}{\kappa_{z_1}}\frac{\partial\sigma_{xz}^{n+1/2}}{\partial z}$$
$$-\frac{\Delta t}{2}\frac{(\alpha_{z_1}\kappa_{z_1}+d_{z_1})}{\kappa_{z_1}}\Psi_{xz_1}^{n+1/2}$$

This was rearranged and then solved for $\Psi_{xz_1}^{n+1/2}$, giving

$$\begin{aligned}&\Psi_{xz_1}^{n+1/2}\\&=\frac{2+\Delta t\alpha_{z_1}}{2\kappa_{z_1}+\Delta t(\alpha_{z_1}\kappa_{z_1}+d_{z_1})}\frac{\partial\sigma_{xz}^{n+1/2}}{\partial z}\\&+\frac{2\kappa_{z_1}}{2\kappa_{z_1}+\Delta t(\alpha_{z_1}\kappa_{z_1}+d_{z_1})}\sum_{p=0}^{n-1}[\frac{\alpha_{z_1}\Delta t}{\kappa_{z_1}}\frac{\partial\sigma_{xz}^{p+1/2}}{\partial z}\\&-\frac{(\alpha_{z_1}\kappa_{z_1}+d_{z_1})\Delta t}{\kappa_{z_1}}\Psi_{xz_1}^{p+1/2}]\end{aligned}\tag{35}$$

The summation term term on the right hand side was then replaced by $\Phi_{xz_1}^{n-1/2}$.

$$\begin{aligned}\Phi_{xz_1}=\sum_{p=0}^{n-1}[&\frac{\alpha_{z_1}\Delta t}{\kappa_{z_1}}\frac{\partial\sigma_{xz}^{p+1/2}}{\partial z}\\&-\frac{(\alpha_{z_1}\kappa_{z_1}+d_{z_1})\Delta t}{\kappa_{z_1}}\Psi_{xz_1}^{p+1/2}]\end{aligned}\tag{36}$$

Physically this held the approximation to the integral at the previous time step. Computationally, this variable was updated after the stresses, velocities and their corresponding correction terms, but at the same time instance. Therefore

$$\begin{aligned}\Psi_{xz_1}^{n+1/2}=&\frac{2+\Delta t\alpha_{z_1}}{2\kappa_{z_1}+\Delta t(\alpha_{z_1}\kappa_{z_1}+d_{z_1})}\frac{\partial\sigma_{xz}^{n+1/2}}{\partial z}\\&+\frac{2\kappa_{z_1}}{2\kappa_{z_1}+\Delta t(\alpha_{z_1}\kappa_{z_1}+d_{z_1})}\Phi_{xz_1}^{n-1/2}\end{aligned}\tag{37}$$

Where $\Phi_{xz_1}^{n+1/2}$ was defined as

$$\Phi_{xz_1}^{n+1/2} = \Phi_{xz_1}^{n-1/2} + \frac{\alpha_{z_1}\Delta t}{\kappa_{z_1}}\frac{\partial \sigma_{xz}^{n+1/2}}{\partial z} - \frac{\Delta t(\alpha_{z_1}\kappa_{z_1} + d_{z_1})}{\kappa_{z_1}}\Psi_{xz_1}^{n+1/2} \tag{38}$$

Calculating the N^{th} order Correction Terms

The next step towards deriving an expression for $J_{xz}^{n+1/2}$ was to eliminate $\Psi_{xz_1}^{n+1/2}$ from the update of $\Phi_{xz_1}^{n+1/2}$. This was done using equations 35 and 38 and resulted in:

$$\Phi_{xz_1}^{n+1/2} = \frac{2\kappa_{z_1} - \Delta t(\alpha_{z_1}\kappa_{z_1} + d_{z_1})}{2\kappa_{z_1} + \Delta t(\alpha_{z_1}\kappa_{z_1} + d_{z_1})}\Phi_{xz_1}^{n-1/2} - \frac{2d_{z_1}\Delta t}{(2\kappa_{z_1} + \Delta t(\alpha_{z_1}\kappa_{z_1} + d_{z_1}))\kappa_{z_1}}\frac{\partial \sigma_{xz}^{n+1/2}}{\partial z} \tag{39}$$

Upon inspection of equation 39, it was found that for $i \in [2, N-1]$, Ψ_{xz_i} could be calculated in an analogous manner to Ψ_{xz_1}, which resulted in

$$\Psi_{xz_i}^{n+1/2} = \frac{2 + \Delta t\alpha_{z_i}}{2\kappa_{z_i} + \Delta t(\alpha_{z_i}\kappa_{z_i} + d_{z_i})}\Psi_{xz_{i-1}}^{n+1/2} + \frac{2\kappa_{z_i}}{2\kappa_{z_i} + \Delta t(\alpha_{z_i}\kappa_{z_i} + d_{z_i})}\Phi_{xz_i}^{n-1/2} \tag{40}$$

Correspondingly, the previous time integrals, Φ_{xz_i} for $i \in [2, N]$ were updated

$$\Phi_{xz_i}^{n+1/2} = \frac{2\kappa_{z_i} - \Delta t(\alpha_{z_i}\kappa_{z_i} + d_{z_i})}{2\kappa_{u_i} + \Delta t(\alpha_{z_i}\kappa_{z_i} + d_{z_i})}\Phi_{xz_i}^{n-1/2} - \frac{2\sigma_{z_i}\Delta t}{(2\kappa_{z_i} + \Delta t(\alpha_{z_i}\kappa_{z_i} + d_{z_i}))\kappa_{z_i}}\Psi_{xz_{i-1}}^{n+1/2} \tag{41}$$

Lastly, using the same methodology as that to arrive at equation 40, equations 29 and 40 were used to create an overall formulation for $J_{xz}^{n+1/2}$

$$J_{xz}^{n+1/2} = \frac{2 + \Delta t\alpha_{z_N}}{2\kappa_{z_N} + \Delta t(\alpha_{z_N}\kappa_{z_N} + d_{z_N})}\Psi_{xz_{N-1}}^{n+1/2} + \frac{2\kappa_{z_N}}{2\kappa_{z_N} + \Delta t(\alpha_{z_N}\kappa_{z_N} + d_{z_N})}\Phi_{xz_N}^{n-1/2} - \frac{\partial \sigma_{xz}^{n+1/2}}{\partial z} \tag{42}$$

From a computational point of view, it should be noted that Ψ_{xz_i} and J_{xz} could be updated within the PML correction loop. This meant that they did not have to be stored in the computer memory, thus minimising the memory requirements.

Implementation of N^{th} order Stretching

Although a formulation for $J_{xz}^{n+1/2}$ had now been calculated, it was not yet in an efficient form to facilitate computation. Further analysis revealed that Ψ_{xz_i} was merely a function of both $\partial\sigma_{xz_1}/\,\partial z$, Φ_{xz_1} and Ψ_{xz_i}. This meant all Ψ_{xz_i} could be eliminated from equation 42. The result was written using a single formula describing the correction term J_{xz} at the current time step. This formulation was finally capable of calculating the stretching functions for a PML of arbitrary order.

$$\begin{aligned} J_{xz}^{n+1/2} = \{(\prod_{q=1}^{N} \mathrm{RA}_{\mathrm{z_q}}) - 1\}\frac{\partial \sigma_{xz}^{n+1/2}}{\partial z} \\ + \sum_{i=1}^{N-1} \{(\prod_{q=i+1}^{N} \mathrm{RA}_{\mathrm{z_q}})\mathrm{RB}_{\mathrm{z_i}}\Phi_{xz}^{n-1/2}\} \\ + \mathrm{RB}_{\mathrm{z_N}}\Phi_{xz_N}^{n-1/2} \end{aligned} \tag{43}$$

where $i \in [2, N-1]$.

Similarly, due to the same relationship between Ψ_{xz_i}, $\partial\sigma_{xz_1}/\,\partial z$ and Φ_{xz_1}, Ψ_{xz_i} was eliminated from the summation memory variable. This yielded

$$\begin{aligned} \Phi_{xz_i}^{n+1/2} = \mathrm{RE}_{\mathrm{z_i}}\Phi_{xz_i}^{n-1/2} - \mathrm{RF}_{\mathrm{z_i}}\{(\prod_{q=1}^{i-1} \mathrm{RA}_{\mathrm{z_q}})\frac{\partial \sigma_{xz}^{n+1/2}}{\partial z} \\ + \sum_{m=1}^{i-1} (\prod_{q=m+1}^{i-1} \mathrm{RA}_{\mathrm{z_q}})\mathrm{RB}_{\mathrm{z_m}}\Phi_{xz_m}^{n-1/2}\} \end{aligned} \tag{44}$$

Where $i \in [2, N-1]$. $\mathrm{RA}_{\mathrm{z}_i}$, $\mathrm{RB}_{\mathrm{z}_i}$, $\mathrm{RE}_{\mathrm{z}_i}$, $\mathrm{RF}_{\mathrm{z}_i}$, were defined by:

$$\begin{aligned} \mathrm{RA}_{\mathrm{z_i}} &= \frac{2 + \Delta t\alpha_{z_i}}{2\kappa_{z_i} + \Delta t(\alpha_{z_i}\kappa_{z_i} + d_{z_i})} \\ \mathrm{RB}_{\mathrm{z_i}} &= \frac{2\kappa_{z_i}}{2\kappa_{z_i} + \Delta t(\alpha_{z_i}\kappa_{z_i} + d_{z_i})} \\ \mathrm{RE}_{\mathrm{z_i}} &= \frac{2\kappa_{z_i} - \Delta t(\alpha_{z_i}\kappa_{z_i} + d_{z_i})}{2\kappa_{z_i} + \Delta t(\alpha_{z_i}\kappa_{z_i} + d_{z_i})} \end{aligned} \tag{45}$$

$$\mathrm{RF}_{\mathrm{z_i}} = \frac{2\sigma_{z_i}\Delta t}{(2\kappa_{z_i} + \Delta t(\alpha_{z_i}\kappa_{z_i} + d_{z_i}))\kappa_{z_i}}$$

Note that only $J_{xz}^{n+1/2}$ and $\Phi_{xz_i}^{n+1/2}$ required updating within the computational time loop. To implement them with the PML scheme they were calculated and updated at each time step and then added to the original FDTD field variables (i.e. equations 14-18). $\mathrm{RA}_{\mathrm{z}_i}$, $\mathrm{RB}_{\mathrm{z}_i}$, $\mathrm{RE}_{\mathrm{z}_i}$, $\mathrm{RF}_{\mathrm{z}_i}$, were not time dependent and therefore could be calculated before the commencement of the integration scheme. Note that due to the nature of PML, the material properties within the PML regions do not require modification, and remain identical to those within the non-PML domain. Additionally, the PML corner regions do not require any additional equations or consideration, thus significantly increasing the ease of programming.

First Order Implementation

Equation 43 described the calculation of the correction term to implement a PML of arbitrary order. If $N = 1$, this formulation reduced to a first order (O1) PML. Note that the first order PML utilised only a single stretching function and mathematically was similar to the one presented by (F. H. Drossaert and Giannopoulos, 2007), (F. Drossaert and Giannopoulos, 2007), albeit with the aforementioned advantages. The formula resulted in

$$J_{xz}^{n+1/2} = \{\mathrm{RA}_{\mathrm{z}_1} - 1\}\frac{\partial \sigma_{xz}^{n+1/2}}{\partial z} + \mathrm{RB}_{\mathrm{z}_1}\Phi_{xz_1}^{n-1/2} \tag{46}$$

followed by the update of $\Phi_{xz_1}^{n+1/2}$

$$\Phi_{xz_1}^{n+1/2} = \mathrm{RE}_{\mathrm{z}_1}\Phi_{xz_1}^{n-1/2} - \mathrm{RF}_{\mathrm{z}_1}\frac{\partial \sigma_{xz}^{n+1/2}}{\partial z} \tag{47}$$

Second Order Implementation

Second order (O2) PML's have been shown to offer increased absorption performance in the field of electromagnetics. Notice that two stretching functions were now required to describe the overall PML attenuation. Inserting $N = 2$ into the correction equation 43 resulted in:

$$J_{xz}^{n+1/2} = \{\mathrm{RA}_{\mathrm{z}_1}\mathrm{RA}_{\mathrm{z}_2} - 1\}\frac{\partial \sigma_{xz}^{n+1/2}}{\partial z} + \mathrm{RA}_{\mathrm{z}_2}\mathrm{RB}_{\mathrm{z}_1}\Phi_{xz_1}^{n-1/2} + \mathrm{RB}_{\mathrm{z}_2}\Phi_{\mathrm{xz}_2}^{n-1/2} \tag{48}$$

which now depended on two updates, for Φ_{xz_2} and Φ_{xz_1}

$$\Phi_{xz_2}^{n+1/2} = \mathrm{RE}_{z_2}\Phi_{xz_2}^{n-1/2} - \mathrm{RF}_{z2}\{\mathrm{RA}_{z_1}\frac{\partial\sigma_{xz}^{n+1/2}}{\partial z} + \mathrm{RB}_{z_1}\Phi_{xz_1}^{n-1/2}\} \tag{49}$$

$$\Phi_{xz_1}^{n+1/2} = \mathrm{RE}_{z_1}\Phi_{xz_1}^{n-1/2} - \mathrm{RF}_{z_1}\frac{\partial\sigma_{xz}^{n+1/2}}{\partial z} \tag{50}$$

Note that although equations 46 and 48, took different forms depending on the order, N, of the PML (i.e first, second...N) RA_{z_i}, RB_{z_i}, RE_{z_i}, RF_{z_i} remained unchanged.

PML Stability

Although it was shown by (Giannopoulos, 2011) that second order PML's can provide enhanced performance over first order PML's for electromagnetic wave absorption, it was still unclear as to whether PML orders greater than second provided any significant benefit. Therefore this work focused primarily upon second order implementation and testing.

The first order stretching functions were written as

$$s_{classical} = \kappa + \frac{d}{i\omega} \tag{51}$$

$$s_{CFS} = \kappa + \frac{d}{\alpha + i\omega} \tag{52}$$

The stretching function of a second order PML depended on the multiplication of two, first order stretching functions. Therefore, considering equations 48 and 6, there were three possible permutations of second order stretching function:

$$s_{classical-classical} = \left(\kappa + \frac{d}{i\omega}\right)\left(\kappa + \frac{d}{i\omega}\right) \tag{53}$$

$$s_{classical-CFS} = \left(\kappa + \frac{d}{i\omega}\right)\left(\kappa + \frac{d}{\alpha + i\omega}\right) \tag{54}$$

$$s_{CFS-CFS} = \left(\kappa + \frac{d}{\alpha + i\omega}\right)\left(\kappa + \frac{d}{\alpha + i\omega}\right) \quad (55)$$

The $s_{classical-classical}$ stretching function was found to offer poor performance due it's limited ability to absorb low frequency waves, and possibly due to the large similarity between first and second order stretching components. Therefore it was discounted from the analysis at an early stage.

The selection of stretching function parameters can have a significant effect on a PML's ability attenuate wave energy. Careless parameter selection can also lead to instability, especially as PML order increases. To meet the stability criterion the real part of the stretching function had to be greater or equal to 1 or the PML caused a physical contraction of space rather than a stretching of space. Similarly, the imaginary part had to be less than or equal to zero or the PML region experienced a magnification of amplitude rather than an attenuation. These relationships were expressed as:

$$r_{O2} \geq 1 \quad (56)$$

And

$$I_{O2} \leq 0 \quad (57)$$

Different second order (and N^{th} order) stretching functions yield different real and imaginary components. Therefore equations 54 and 55 were analysed to determine appropriate parameter selections to meet the conditions outlined in equations 56 and 57. Despite this, it should be noted that in cases where the stability criteria are not met, it doesn't not necessarily guarantee that errors will be introduced into the solution.

Classical-CFS Stability Criterion

(Giannopoulos, 2011) found that for the absorption of electromagnetic waves, optimum performance was achieved by combining classical and CFS stretching functions (equation 54). It was postulated that for some domains, combining the classical PML's ability to absorb frequency independent waves with the CFS-PML's ability to absorb low frequency evanescent waves, greater performance was achievable. For the elastodynamics case, the real and imaginary components of the 'classical-CFS' case were found to be:

$$r_{O2} = \kappa_2 + \frac{d_2\alpha_2}{\alpha_2^2 + \omega^2} - \frac{d_1 d_2}{\alpha_2^2 + \omega^2} \quad (58)$$

$$I_{O2} = \frac{d_1\kappa_2}{\omega} + \frac{d_2\omega}{\alpha_2^2 + \omega^2} + \frac{d_1 d_2 \alpha_2}{\omega(\alpha_2^2 + \omega^2)} \quad (59)$$

CFS-CFS Stability Criterion

The CFS-CFS PML approach had a greater number of degrees of freedom in comparison to the RI-CFS-PML because additional α and κ coefficients were utilised. In fact, the classical-CFS formulation can be considered a subset of the CFS-CFS formulation. Therefore the CFS-CFS PML was likely to provide enhanced absorption.

The real and imaginary parts of the CFS-CFS stretching function were found to be:

$$r_{O2} = \kappa_1\kappa_2 + \frac{\alpha_2\kappa_1 d_2}{\alpha_2^2+\omega^2} + \frac{\alpha_1\kappa_2 d_1}{\alpha_1^2+\omega^2} + \left(\frac{\alpha_1\alpha_2}{(\alpha_1^2+j\omega^2)(\alpha_2^2+j\omega^2)} - \frac{\omega^2}{(\alpha_1^2+j\omega^2)(\alpha_2^2+j\omega^2)}\right) d_1 d_2 \tag{60}$$

$$I_{O2} = \frac{\kappa_1\omega d_2}{(\alpha_2^2+j\omega^2)} + \frac{d_1\omega\kappa_2}{(\alpha_1^2+\mathrm{j}\omega^2)} - \left(\frac{\alpha_2\omega}{(\alpha_1^2+\omega^2)(\alpha_2^2+\omega^2)} + \frac{\alpha_1\omega}{(\alpha_1^2+\omega^2)(\alpha_2^2+\omega^2)}\right) d_1 d_2 \tag{61}$$

Assuming that all PML coefficient values were chosen to be positive, the imaginary part of the stretching function would always be fulfilled. Despite this, unlike the classical-CFS case, the stability of the real part of the CFS-CFS stretching function was frequency dependant. Therefore to maintain stability, $\alpha_1\alpha_2 > \omega^2$, and $\kappa_2 \geq 1$.

Unlike the Classical-CFS stretching function, α_2 scaling had to be considered relative to α_1 scaling to ensure that the stability criterion was met at every grid point within the PML region. If both α_1 and α_2 were scaled from a minimum at the threshold between PML and modelling space, to a maximum at the PML extremity then it was more straightforward to ensure the stability condition was met.

Although the CFS-CFS stability criterion was slightly more challenging to meet, in comparison to the classical-CFS case, it offered five more dof's to aid absorption.

NUMERICAL RESULTS

Example 1 - Square 2D Homogenous Full-Space

Problem Formulation

The performance of the new correction PML formulation in comparison to a traditional non-correction approach was compared using a square two dimensional homogenous full space, as also used by (F. H. Drossaert and Giannopoulos, 2007). The domain was 77.5m in length in both x and z directions with a cell size of 0.25m (Figure 1). A rotated staggered grid (RSG) stencil was used to describe the staggered nature of the velocity and stress components. The central differencing time integration scheme was second order accurate in both space and time. The material properties were $\rho = 2000kg/m^3$, $\lambda = 500$ MPa and $\mu = 300$ MPa. The central grid point (155,155) was excited using a pulse in the shape of the second derivative of a gaussian, with frequency 20Hz. The receiver was offset from the upper left corner by 5m in both directions.

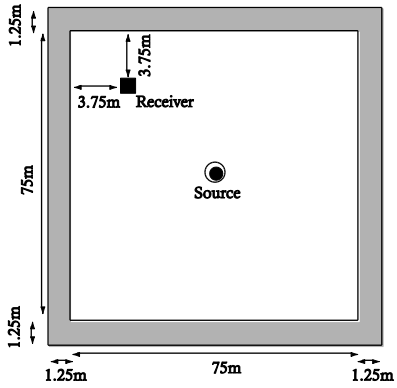

Figure 1 - Example 1 schematic

Model Results - Correction RI-PML Vs Non-Correction RI-PML

To compare the performance of the new correction PML, it's performance was tested against an alternative PML implementation, using Example 1. To create the alternative first order PML scheme, (F. H. Drossaert and Giannopoulos, 2007) was used. To create the correction PML, equations 46 and 47 were used. A key difference in the approaches was that the non-correction formulation required direct manipulation of the underlying velocity/stress update equations. The correction PML equations did not require such manipulation and took the time domain form:

$$v_x = b\left(\frac{\partial \sigma_{xx}}{\partial x} + \frac{\partial \sigma_{xz}}{\partial z}\right) + PML_{v_x} \tag{62}$$

$$v_z = b\left(\frac{\partial \tilde{\sigma}_{xz}}{\partial x} + \frac{\partial \sigma_{zz}}{\partial z}\right) + PML_{v_z} \quad (63)$$

$$\sigma_{xx} = (\lambda + 2\mu)\frac{\partial v_x}{\partial x} + \lambda\frac{\partial v_z}{\partial z} + PML_{\sigma_{xx}} \quad (64)$$

$$\sigma_{zz} = (\lambda + 2\mu)\frac{\partial v_z}{\partial z} + \lambda\frac{\partial v_x}{\partial x} + PML_{\sigma_{zz}} \quad (65)$$

$$\sigma_{xz} = \mu\left(\frac{\partial v_z}{\partial x} + \frac{\partial v_x}{\partial z}\right) + PML_{\sigma_{xz}} \quad (66)$$

with the correction coefficients calculated in the PML zones as

$$PML_{v_x} = b(J_{xx} + J_{xz}) \quad (67)$$

$$PML_{v_z} = b(J_{xz} + J_{zz}) \quad (68)$$

$$PML_{\sigma_{xx}} = (\lambda + 2\mu)M_{xx} + \lambda M_{xz} \quad (69)$$

$$PML_{\sigma_{zz}} = (\lambda + 2\mu)M_{zz} + \lambda M_{zx} \quad (70)$$

$$PML_{\sigma_{xz}} = \mu(M_{zx} + M_{xz}) \quad (71)$$

J_{xu} and M_{xu} were calculated as described by equations 19 and 20. The regions for the calculation of the PML correction terms could also be written as:

$$PML_{u_i} \neq 0 \quad \text{for} \quad x \in [0 - 1.25, 76.25 - 77.5] \quad (72)$$

$$z \in [0 - 1.25, 76.25 - 77.5] \quad (73)$$

$$PML_{u_i} = 0 \quad \text{for} \quad x \in [1.25 - 76.25] \quad (74)$$

$$z \in [1.25 - 76.25] \quad (75)$$

For both tests the PML was five cells thick and for simplicity, first order classical stretching functions (equation 51) were compared (i.e. $\kappa_{max} = 1$ and $\alpha_{max} = 0$). d_{max} was calculated in accordance with (Collino and Tsogka, 2001), and d was scaled quadratically with d_{max} located at the extremity of the computational grid. The calculation of d_{max} is shown in equation 76, where v_p was the compressional wave velocity, L was the PML depth and R was the reflection coefficient (1×10^{-5})(Collino and Tsogka, 2001) . It should also be noted that the RSG was found to make the implementation of both PML's more straightforward than other grid types due to the co-location of velocity components, and the co-location of stress components.

$$d_{max} = \frac{3v_p}{2L} log \frac{1}{R} \tag{76}$$

Figure 2 shows the resulting traces for both schemes. It was found that the performance of both PML's was so similar that the trace time histories were not useful for enabling comparison. Therefore the difference between each trace at each timestep was also plotted and is shown in Figure 3. It can be seen that the error was in the order of $1x10^{-15}$, with a maximum of $2x10^{-15}$. Lastly, a commonly used error metric (equation 77) was used to calculate the difference between traces. Figure 4 shows that the resulting error was in the region of -300dB.

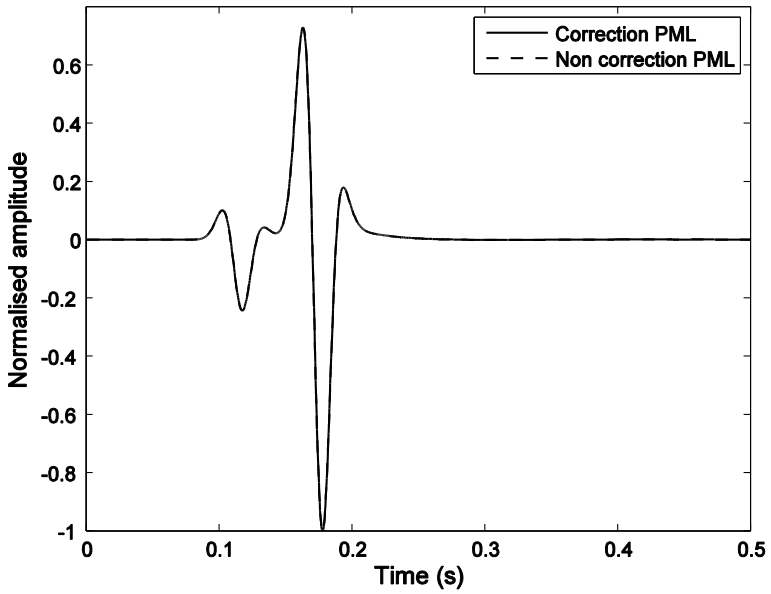

Figure 2 - Example 1 - trace history

$$\begin{aligned} &\text{Error}_{\text{db}}|_{i,j}^{n} \\ &= 20\log_{10} \frac{\| E_{\text{correction}}|_{i,j}^{n} - E_{\text{non-correction}}|_{i,j}^{n} \|}{\| E_{\text{non-correction}_{\text{max}}}|_{i,j} \|} \end{aligned} \tag{77}$$

Note that $E_{\text{correction}}|_{i,j}^{n}$ represented the correction PML trace at a point in time, n, and at spatial location, i, j. $E_{\text{non-correction}}|_{i,j}^{n}$ represented the non-correction PML solution, and $E_{\text{non-correction}_{\text{max}}}$ was the maximum amplitude of the non-correction PML trace. When plotted this allows for a better visual interpretation of the errors at each point in time.

Therefore it was concluded that the new correction implementation performed nearly identically to the original non-correction PML. The discrepancies were in the range of (1 x 10^{-15}) or -300dB, which although theoretically should have been zero, were insignificant and most likely generated by numerical precision errors (e.g. rounding errors associated with the computer, etc).

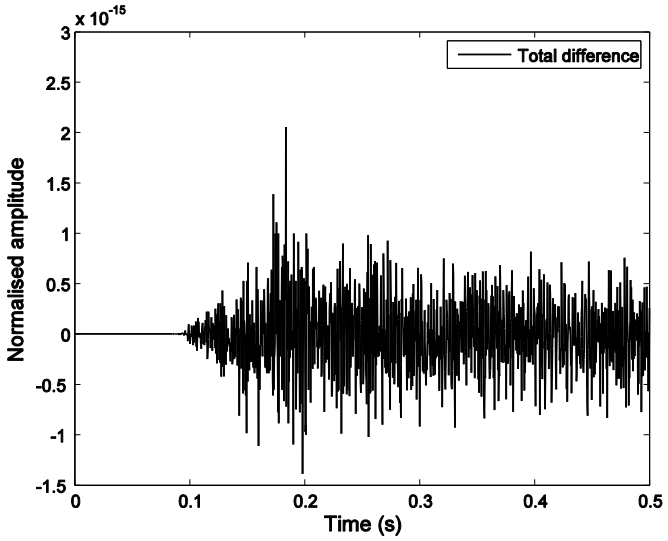

Figure 3 - Example 1 - trace error time history

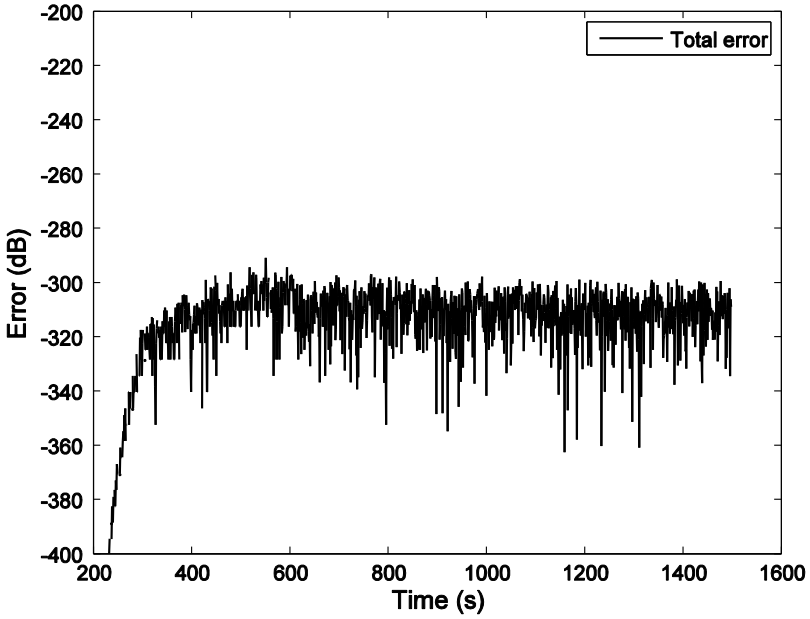

Figure 4 - Example 1 - error time history

Example 2 - Rectangular 2D Homogenous Full-Space

Problem Formulation

Elongated rectangular domains can reduce the absorption performance of PML's. Therefore two PML comparisons were undertaken. Firstly, the new first order recursive integration correction PML was compared to an alternative PML implementation based on a convolution approach. Secondly, the new higher order correction PML was compared to a first order correction PML approach.

The grid used for comparison was identical to that outlined in (Martin et al., 2010) and (Komatitsch and Martin, 2007) with 101 x 641 square cells and 10m spacing between grid points in both directions (Figure 5). The homogenous material was characterised by pressure wave velocity $c_p = 3300\ ms^{-1}$, shear wave velocity $c_s = 1905\ ms^{-1}$ and density $\rho = 2800\ \text{kg}m^{-3}$. The computational scheme was second order accurate in both space and time with a constant time step of $\delta t = 0.001s$. The staggered grid stencil followed that outlined by (Virieux, 1986) and was bounded on all sides by a PML region 10 cells thick.

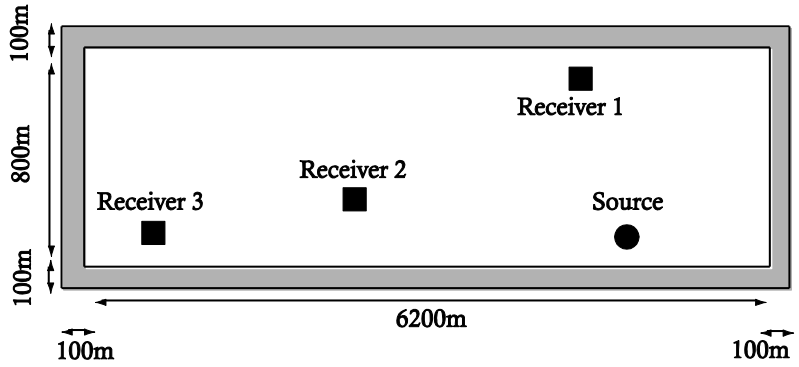

Figure 5 - Example 2 - model schematic (rotated 90 degrees)

A 8Hz excitation with the form of a first derivative of a gaussian was used to excite the velocity components in both horizontal and vertical directions at coordinate (79, 427). Receivers one, two and three were placed at (20,413), (70,227) and (81,27) respectively. Physically receiver one was located closest to the source and receiver three located furthest away. At each receiver, both horizontal and vertical velocity time histories were recorded.

Example 2 (Test 2.1) - Correction RI-PML vs C-PML

For the domain shown inFigure 5, (Martin et al., 2010) previously found a set of high performance absorption coefficients. Values for κ_{max} and α_{max} are shown in equations 78 and 79 ($\omega =$ excitation frequency) and α was scaled linearly with a maximum at the edge of the computational grid (Festa and Vilotte, 2005). d_{max} and the profile for d were calculated using the recommendations outlined in (Collino and Monk, 1998). Therefore the same coefficients were for the first order correction PML, based on a recursive integration approach, and for the C-PML.

$$\kappa_{max} = 7 \tag{78}$$

$$(\alpha\_max = \omega\pi) \tag{78}$$

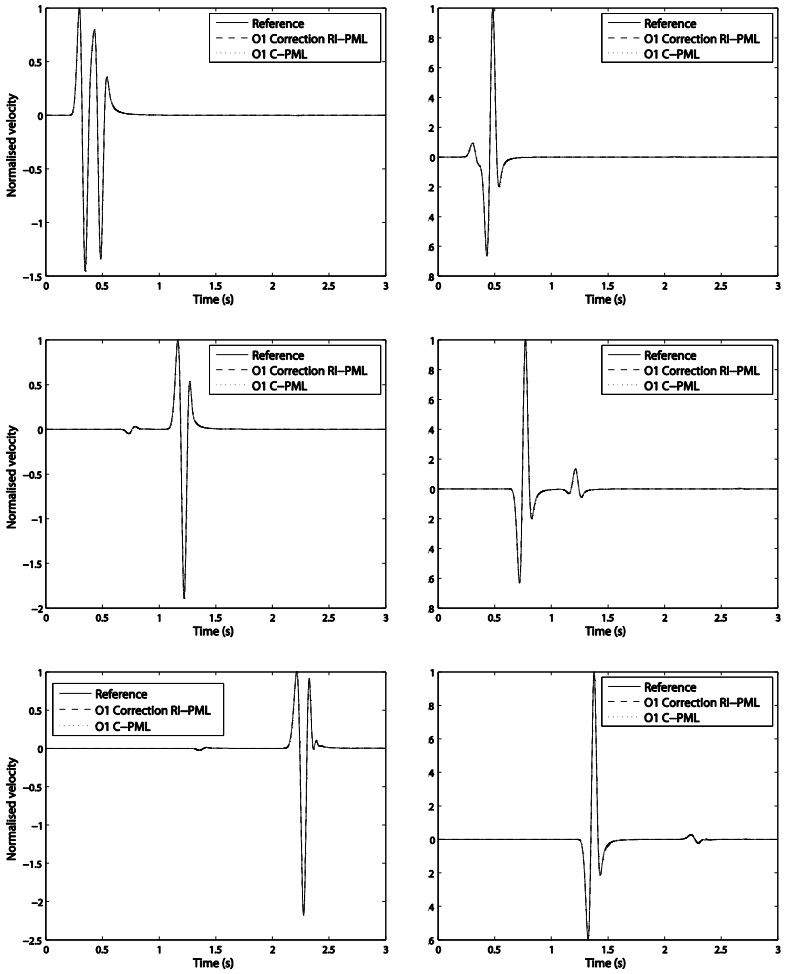

Figure 6 - Trace comparisons - RI-PML vs C-PML, Top left: v_x receiver 1, Top right: v_z receiver 1, Middle left: v_x receiver 2, Middle right: v_z receiver 2, Bottom left: v_x receiver 3, Bottom right: v_z receiver 3

Figure 6 shows that the resulting traces for both PML conditions were similar. Therefore, once again, to facilitate a more detailed comparison of performance, a log based metric was introduced. Note that this time the error was calculated for the performance of each PML compared to a reference solution, rather than directly between the PML formulations.

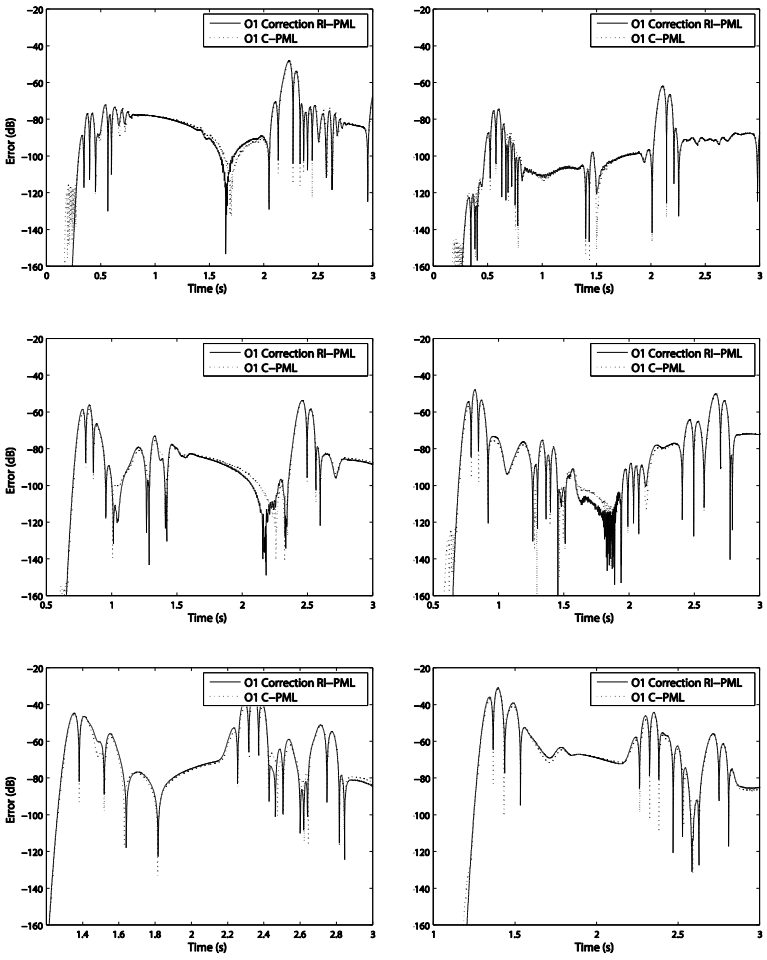

Figure 7 - Error comparisons - RI-PML vs C-PML, Top left: v_x receiver 1, Top right: v_z receiver 1, Middle left: v_x receiver 2, Middle right: v_z receiver 2, Bottom left: v_x receiver 3, Bottom right: v_z receiver 3

$$\text{Error}_{\text{db}}|_{i,j}^{n} = 20\log_{10}\frac{\| E|_{i,j}^{n} - E_{\text{ref}}|_{i,j}^{n} \|}{\| E_{\text{ref}_{\text{max}}}|_{i,j} \|} \tag{79}$$

Although the error plots (Figure 7) allowed for easier comparison between traces, there were still large similarities between results. At some points the CPML was found to perform marginally better but at other points the correction PML exhibited slightly higher

accuracy. This was evident at all receivers. Therefore it was concluded that the correction PML offered very similar performance to the CPML implementation. Despite this, due to the recursive integration scheme used for the RI-PML, if offered a solution with reduced memory requirements.

Example 2 (Test 2.2) - First Order PML vs Second Order PML

A Practical Approach To Optimisation

An advantage of using a higher order PML in comparison to a first order PML was that there were a greater number of parameters that could be altered to optimise absorption. A challenge associated with these extra degrees of freedom was that each one had to be carefully chosen to maximise absorption and meet stability criteria. This task can be time consuming.

For example, first considering the stretching function associated with the original first order classical PML (equation 51), it had only two modifiable degrees of freedom (d_{max} and the polynomial scaling order for d). This made the optimisation process relatively straightforward. In comparison, the alternative CFS-PML stretching function had seven degrees of freedom, including d_{max}, κ_{max}, α_{max}, and the polynomial scaling of d, κ, α. Additionally, assuming that d and κ were always scaled with a maximum at the edge of the computational grid, but α could be scaled in either direction, this created one extra dof. This dof described the scaling direction.

Then, considering higher order stretching functions it was clear that the number of dof's would increase even further. For example, regarding a second order PML, the classical-CFS PML stretching function (equation 54) had 9 dof's and the CFS-CFS stretching function (equation 55) had 14 dof's. Therefore it became clear that the optimisation task required for the overall stretching function was onerous. If N_{dof} = number of dof's within a stretching function, then the total number of dof's needed to describe a PML made up from a number, $Classical_n$, of classical stretching functions and a number, CFS_n, of CFS stretching functions was:

$$N_{dof} = 2Classical_n + 7CFS_n \tag{80}$$

This aim of this work was to present the new formulations for both the first order correction PML and the higher order PML. It was also to show that the higher order PML formulation was capable of offering absorption benefits over traditional first order approaches. Despite this, it was not intended to investigate approaches to the optimisation of higher order PML coefficients – instead, as an initial investigation, a trial-and-error

approach to optimisation was used exclusively (for all examples presented in this work). PML coefficient optimisation is an active and ongoing area of research and as such it is anticipated that new developments will allow for the efficient optimisation of PML coefficients, thus increasing the performance and competitiveness of higher order formulations in comparison to first order PMLs.

Therefore, an attempt was made to show that the higher order PML was capable of outperforming first order schemes while minimising the number of dof's required for optimisation. This was achieved by using test examples from the literature where the original authors had already determined the optimum first order parameters. These parameters were then combined with a second set of CFS parameters to create a second order CFS-CFS stretching function. This meant that the higher order PML performance could be investigated while optimising only a reduced number of coefficients. It also provided a conclusive method to test whether the second order PML offered enhanced performance over the first order PML.

Second Order PML vs First Order PML

To test the ability of a higher order PML scheme to outperform its first order counterpart, the example outlined by (Martin et al., 2010) was also used. The original optimised stretching function coefficients as outlined by (Martin et al., 2010) were used to describe the first order CFS stretching component. This was then combined with another CFS stretching function, as described by (equation 55) to create a second order CFS-CFS stretching function. The time domain equations were identical to those presented in equations 62-66, however the correction PML terms (i.e. J_{xu}) were modified to include the second order CFS-CFS stretching function (equations 48 and 55).

The second set of CFS parameters were as follows:

$$d_{max_2} = \frac{d_{max_1}}{30} \tag{81}$$

$$\kappa_{max_2} = 1.5 \tag{82}$$

$$\alpha_{max_2} = 2d_{max_1} \tag{83}$$

It should also be noted that d_2 and κ_2 were scaled using second order polynomials and that α_2 was scaled linearly.

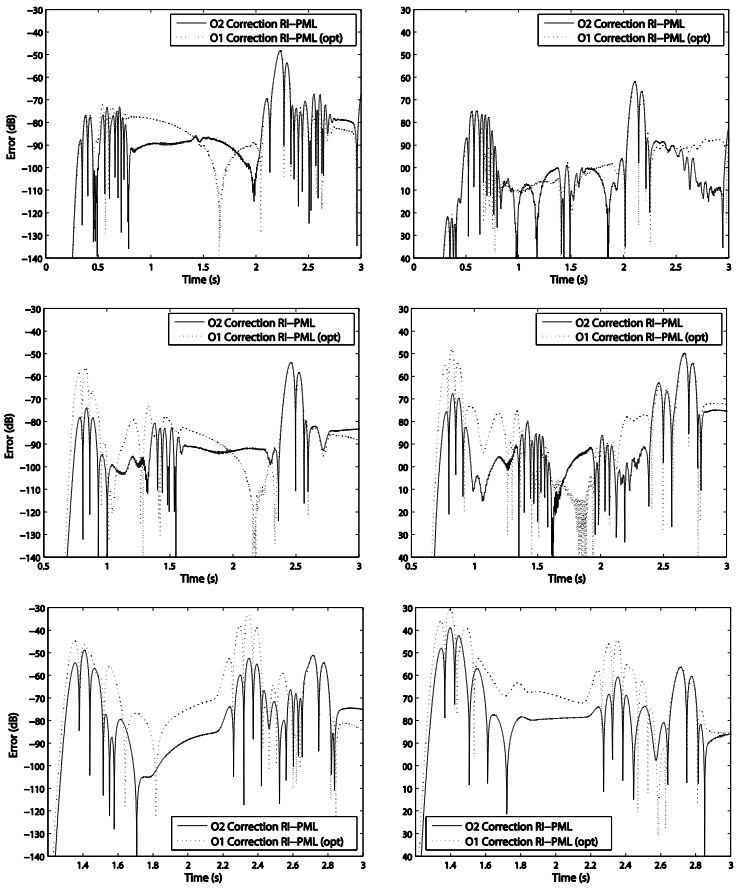

Figure 8 - Error comparisons - First order PML vs Second order PML, Top left: ν_x receiver 1, Top right: ν_z receiver 1, Middle left: ν_x receiver 2, Middle right: ν_z receiver 2, Bottom left: ν_x receiver 3, Bottom right: ν_z receiver 3

Figure 8 shows the resulting error plots. Both first order CFS formulations produced nearly identical results and it was found that the overall error increased as the receiver distance was increased. Concerning the O2 CFS-CFS implementation, performance at receivers vx_1 and vz_1 was improved slightly but as distance increased, performance benefit increased rapidly in comparison to the O1 scheme. Receivers vx_3 and vz_3 showed a marked improvement with on average between 10dB and 20dB less error.

The furthest away receivers were subject to a greater number of evanescent waves in comparison to the closest receivers. PML schemes typically have degraded performance under such conditions but the additional degrees of freedom associated with the O2 PML allowed it to maintain higher levels of performance in comparison to both CFS stretching functions.

As the close receivers experienced only a low percentage of these waves the first order CFS was also capable of high performance absorption. Therefore there was not much scope for improvement by adding an additional stretching function.

It should be noted that attempts were also made to improve absorption performance using the classical-CFS stretching function. Despite this, for this particular full-space model no significant performance benefits were found.

Investigations were also performed to compare the computational performance between the first and second order PML's. Simulations were performed using MATLAB, running on a laptop PC with a 2.66 GHz processor and 4GB of RAM. The computational time taken for the first order test case to run was 91s, whereas the second order test case took 140s. Therefore when considering the deployment of a higher order PML, it is important that the potential absorption benefit justifies the increase in computational resource. One possible application is the use of a hybrid (01-02) PML where all model edges except those subject to a large percentage of evanescent waves are subject to a first order PML, while the the remaining sides are terminated using a second order PML. Depending on the domain under consideration, this potentially has the ability to offer increased absorption with minimised run times.

Another consideration is that programming the extra equations/fields associated with the higher order PML requires additional time and effort. Thus, it must also be considered whether this extra effort is better spent modifing an existing first order implementation (e.g. increasing the physical thickness of the PML), rather than programming a higher order PML.

Therefore, in conclusion, due to the increased performance, particularly at large offsets, the second order PML offered a additional absorption in comparison to its first order alternative. Despite this, the second order PML required additional computational resources and programming effort.

Example 3 - A Rectangular 2D Homogenous Half-Space

Test 3.1 - Second Order PML vs First Order PML

For relatively near surface seismic applications such as earthquake engineering it is common to perform simulations in the presence of a free surface boundary condition. Such models generate wave fields that are more complex than full-space models. These wave fields include surface waves in the form of exponentially decaying Rayleigh waves, which can present challenges for absorbing boundary conditions (Zeng et al., 2011).

To test the ability of the higher order PML to absorb surface waves, a near surface model was replicated from (F. Drossaert and Giannopoulos, 2007). This elongated domain had dimensions 3750m x 250m with cell size 2.5m and a time step of 3.2 ms. The source and receiver were placed 2125m apart to test the ability of the PML to absorb evanescent waves subject to large grazing angles.

The free surface was achieved by setting the density and shear wave velocity of the five cells above the free surface close to zero. A rotated staggered grid, with second order accuracy in both space and time, was used to describe the velocity and stress discretisation. The use of the RSG facilitated a straightforward implementation of the free surface because only density values had to be averaged across the interface. Excitation was provided by a Gaussian shaped impulse (centre frequency 1.5Hz) in the vertical direction. The material properties of the medium were, $\rho = 2000kg/m^3$, $\lambda = 600MPa$ and $\mu = 300MPa$.

The PML zones truncated three sides of the grid, with the vertical sides terminating at the free surface as shown in Figure 9. The optimal PML coefficients for the domain, as previously found by (F. Drossaert and Giannopoulos, 2007) were $\sigma_{max} = 234.2$, $\kappa_{max} = 25$ and $\alpha_{max} = 10$. All attenuation parameters were scaled using a second order polynomial function, however α_{max} was scaled inversely meaning it had a value of 0 at the extremity of the grid. Once again a large reference model was used to assess PML performance.

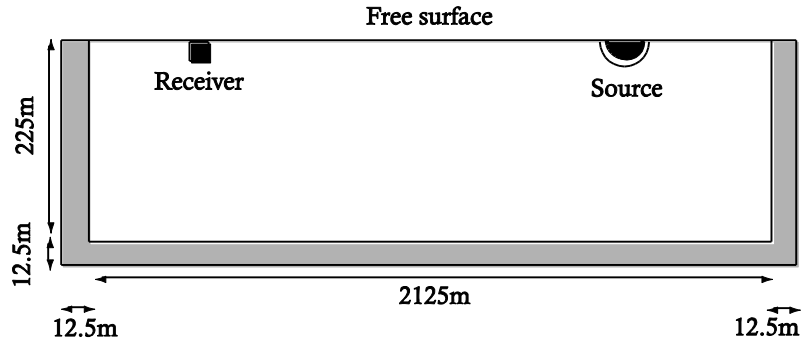

Figure 9 - Example 3 - model schematic

A stretching function with form $s_{CFS-CFS}$ was used, with parameters:

$$d_{max_2} = 50 d_{max_1} \quad (84)$$

$$\kappa_{max_2} = 1 \quad (85)$$

$$\alpha_{max_2} = 800 \quad (86)$$

Note that α_2 was scaled linearly, also with a minimum at the extremity of the grid. d_2 was scaled in the same manner as d_1.

Figure 10 shows the resulting vertical velocity error for the surface receiver. It was found that that the maximum error occurred approximately at 6.5 seconds with the first order PML generating an error of -11.5 dB. In comparison, the second order PML reduced this error by -11.5 dB to a total of -23 dB. At the time steps before the maximum error, the second order PML was found to offer a slight improvement in performance whereas after the maximum error, it was found to offer a slight decrease in absorption. Despite this, the overall error was lower and the error profile was flatter indicating an overall improvement in performance.

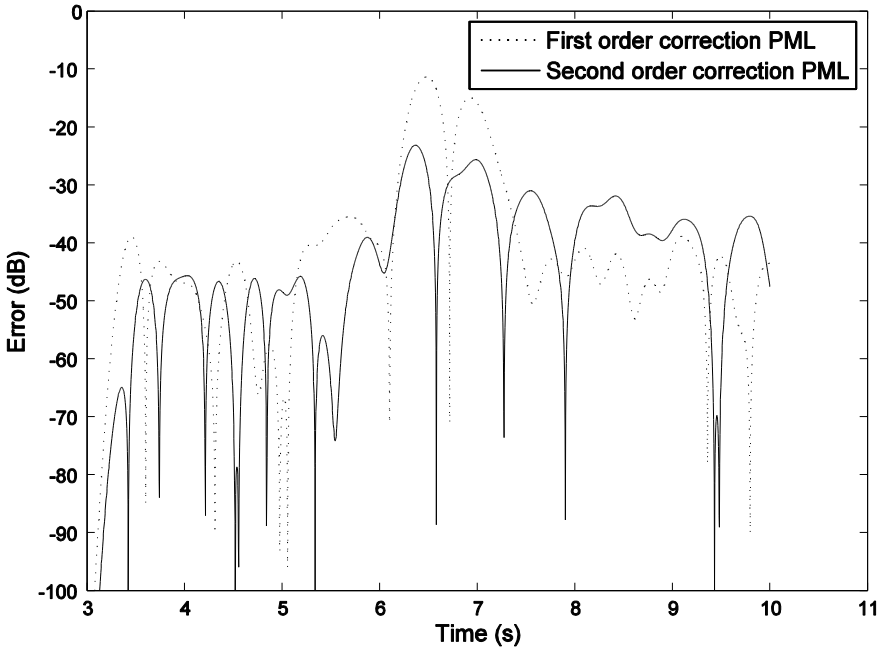

Figure 10 - Example 3 - error

CONCLUSIONS

Two new unsplit PML formulations were presented for the absorption of seismic wave energy. Both formulations were designed for implementation within arbitrary space/time integration schemes and arbitrary FDTD stencils.

The initial was a first order 'correction' approach that used correction terms to adjust the traditional FDTD update equations, thus simulating PML attenuation. As the correction PML did not require any modification of the traditional FDTD update equations, it greatly reduced the programming complexity of PML implementation. The advantages of using a correction PML over traditional PML implementations were found to be:

1. It increased the ease of PML implementation
2. It could be added to existing codes without making any changes to the underlying update equations
3. It offered seamless absorption in model corner regions without any special consideration
4. It had identical absorption performance to traditional PML implementations
5. It allowed for the implementation of arbitrary stretching functions, thus making the implementation of higher order PML's straightforward
6. It's recursive integration approach required less memory storage than alternative approaches, thus reducing computational requirements

More importantly, in addition to the correction PML, a formulation to create higher order PML's, of arbitrary order, was presented. To assess the ability of the new PML formulation to increase absorption, two examples were outlined. One example was an elongated rectangular full-space and the other an elongated rectangular half-space. The key findings were:

1. Second order PML's offer an increased number of degrees of freedom in comparison to first order schemes ,thus facilitating superior absorption performance.
2. Higher order PML's require careful attenuation coefficient selection to maximise absorption and maintain PML stability
3. Higher order PML's require additional computational resources in comparison to first order schemes. This additional computational cost must be carefully considered when selecting an appropriate PML formulation.

ACKNOWLEDGEMENTS

The authors would like to acknowledge the facilities provided by the University of Edinburgh and Heriot-Watt University. Without these resources this work would not have been possible.

REFERENCES

Abarbanel, S., Gottlieb, D., 1997. A Mathematical Analysis of the PML Method. J. Comput. Phys. 134, 357–363. doi:10.1006/jcph.1997.5717

Basu, U., 2009. Explicit finite element perfectly matched layer for transient three-dimensional elastic waves. Int. J. Numer. Methods Eng. 77, 151–176. doi:10.1002/nme

Basu, U., Chopra, A.K., 2004. Perfectly matched layers for transient elastodynamics of unbounded domains. Int. J. Numer. Methods Eng. 59, 1039–1074.

Becache, E., Ezziani, A., Joly, P., 2003. Mathematical and Numerical Modeling of Wave Popagation in Linear Viscoelastic Media, in: Mathematical and Numerical Aspects of Wave Propagation. pp. 916–921.

Berenger, J., 1996. A perfectly matched layer for free-space simulation in finite-difference computer codes. Ann. Des Télécommunications 51, 39–46.

Berenger, J.P., 1994. A perfectly matched layer for the absorption of electromagnetic waves. J. Comput. Phys. 114, 185–200. doi:10.1006/jcph.1994.1159

Cerjan, C., Kosloff, D., Kosloff, R., Resheq, M., 1985. A nonreflecting boundary condition for discrete acoustic and elastic wave equations. Geophysics 50, 705–708.

Chew, W., Lui, Q., 1996. Perfectly Matched Layers for Elastodynamics: A New Absorbing Boundary Condition. J. Comput. Acoust. 4, 341–359.

Chew, W., Weedon, W., 1994. A 3D perfectly matched medium from modified maxwell's equations with stretched coordinates. Microw. Opt. Technol. Lett. 7, 599–604.

Collino, F., Monk, P., 1998. Optimising the perfectly matched layer. Appl. Mech. Eng. 164, 157–171.

Collino, F., Tsogka, C., 2001. Application of the perfectly matched absorbing layer model to the linear elastodynamic problem in anisotropic heterogeneous media. Geophysics 66, 294–307.

Correia, D., Jin, J., 2005. On the Development of a Higher-Order PML. IEEE Trans. Antennas Propag. 53, 4157–4163.

Drossaert, F., Giannopoulos, A., 2007. Complex frequency shifted convolution PML for FDTD modelling of elastic waves. Wave Motion 44, 593–604. doi:10.1016/j.wavemoti.2007.03.003

Drossaert, F.H., Giannopoulos, A., 2007. A nonsplit complex frequency-shifted PML based on recursive integration for FDTD modeling of elastic waves. Geophysics 72, T9. doi:10.1190/1.2424888

Festa, G., Vilotte, J., 2005. The Newmark scheme as velocity–stress time-staggering: an efficient PML implementation for spectral element simulations of elastodynamics. Geophys. J. Int. 161, 789–812.

Giannopoulos, A., 2011. Unsplit implementation of Higher-Order PMLs. IEEE Trans. Antennas Propag. 1–7.

Graves, R.W., 1996. Simulating Seismic Wave Propagation in 3D Elastic Media Using Staggered-Grid Finite Differences. Bull. Seismol. Soc. Am. 86, 1091–1106.

Guddati, M.N., Lim, K., 2006. Continued fraction absorbing boundary conditions for convex polygonal domains. Int. J. Numer. Methods Eng. 66, 949–977.

Hagstrom, T., Hariharan, S.I., 1998. A formulation of asymptotic and exact boundary conditions using local operators. Appl. Numer. Math. 27, 403–416.

Hastings, F., Schneider, J.B., Broschat, S.L., 1996. Application of the perfectly matched layer (PML) absorbing boundary condition to elastic wave propagation. J. Acoust. Soc. Am. 100, 3061–3069.

Higdon, R.L., 1986. Absorbing Boundary Conditions for Difference Approximations to the Multi-Dimensional Wave Equation. Math. Comput. 47, 437. doi:10.2307/2008166

Komatitsch, D., Martin, R., 2007. An unsplit convolutional perfectly matched layer improved at grazing incidence for the seismic wave equation. Geophysics 72, SM155–SM167. doi:10.1190/1.2757586

Kouroussis, G., Parys, L. Van, Conti, C., Verlinden, O., 2014. Using three-dimensional finite element analysis in time domain to model railway-induced ground vibrations. Adv. Eng. Softw. 70, 63–76.

Kouroussis, G., Verlinden, O., Conti, C., 2011. Finite-Dynamic Model for Infinite Media: Corrected Solution of Viscous Boundary Efficiency. ASCE J. Eng. Mech. 137, 509–511. doi:10.1061/(ASCE)EM.1943-7889.0000250.

Kuzuoglu, M., Mittra, R., 1996. Frequency dependence of the constitutive parameters of causal perfectly matched anisotropic absorbers. Microw. Guid. Wave Lett. 6, 447–449.

Laghrouche, O., Le Houédec, D., 1994. Soil–railway interaction for active isolation of traffic vibration. Adv. Simul. Interact. Tech. 31–36.

Lysmer, J., Kuhlemeyer, R., 1969. Finite dynamic model for infinite media. J. Eng. Mech. 859–877.

Martin, R., Komatitsch, D., Ezziani, A., 2008. An unsplit convolution perfectly matched layer improved at grazing incidence for seismic wave propagation in poroelastic media. Geophysics 73, T51–T61.

Martin, R., Komatitsch, D., Gedney, S.D., Bruthiaux, E., 2010. A High-Order Time and Space Formulation of the Unsplit Perfectly Matched Layer for the Seismic Wave Equation Using Auxiliary Differential Equations (ADE-PML). Comput. Model. Eng. Sci. 56, 17–40.

Peng, C., Toksoz, M., 1995. An optimal absorbing boundary condition for elastic wave modeling. Geophysics 60, 296–301.

Roden, J.A., Gedney, S.D., 2000. Convolutional PML (CPML): An efficient FDTD implementation of the CFS-PML for arbitrary media. Microw. Opt. Technol. Lett. 27, 334–339.

Virieux, J., 1986. P-SV wave propagation in heterogenous media: Velocity-stress finite-difference method. Geophysics 51.

Zeng, C., Xia, J., Miller, J., Tsoflias, G., 2011. Application of the multiaxial perfectly matched layer (M-PML) to near-surface seismic modeling with Rayleigh waves. Geophysics 76, T43–T52.

Zhang, W., Shen, Y., 2010. Unsplit complex frequency-shifted PML implementation using auxiliary differential equations for seismic wave modeling. Geophysics 75, T141–T154. doi:10.1190/1.3463431

APPENDIX - HIGHER ORDER PML'S FOR A GENERAL 3D CASE

For a staggered scheme where velocity components are updated at $t = n$ and stress components are updated at $t = n + 1/2$, the calculation of velocity for the entire grid is as follows:

$$v_i^n = v_i^{n-1} + b\delta t(J_{ii}^n + J_{ij}^n + J_{ik}^n) \tag{87}$$

where δt is the time step size and $i, j, k \in [x, y, z]$. The PML velocity correction terms J_{ii}, J_{ij}, J_{ik} are calculated using

$$\begin{aligned} J_{ij}^n = &\{(\prod_{q=1}^{N} \mathrm{RA_{j_q}}) - 1\}\frac{\partial d_{ij}^n}{\partial j} + \\ &\sum_{p=1}^{N-1} \{(\prod_{q=p+1}^{N} \mathrm{RA_{j_q}})\mathrm{RB_{j_p}}\Phi_{ij}^{n-1}\} + \mathrm{RB_{j_N}}\Phi_{ij_N}^{n-1} \end{aligned} \tag{88}$$

where N is the order of PML and $p \in [1, N]$. The previous time integral $\Phi_{ij_p}^n$ is obtained through

$$\begin{aligned} \Phi_{ij_p}^n = &\mathrm{RE_{j_p}}\Phi_{ij_p}^{n-1} - \mathrm{RF_{j_p}}\{(\prod_{q=1}^{p-1} \mathrm{RA_{j_q}})\frac{\partial d_{ij}^n}{\partial j} + \\ &\sum_{m=1}^{p-1} (\prod_{q=m+1}^{p-1} \mathrm{RA_{j_q}})\mathrm{RB_{j_m}}\Phi_{ij_m}^{n-1}\} \end{aligned} \tag{89}$$

Similarly, stresses at $t = n + 1/2$ can then be calculated using

$$\begin{aligned} d_{ij}^{n+1/2} = d_{ij}^{n+1/2} + \delta t C_{ijkl}(M_{i\square}^{n+1/2} + M_{ij}^{n+1/2} \\ + M_{ik}^{n+1/2}) \end{aligned} \tag{90}$$

with the correction terms found using

$$\begin{aligned} \mathrm{M}_{ij}^{n+1/2} = &\{(\prod_{q=1}^{N} \mathrm{RA_{j_q}}) - 1\}\frac{\partial v_j^{n+1/2}}{\partial j} + \\ &\sum_{p=1}^{N-1} \{(\prod_{q=p+1}^{N} \mathrm{RA_{j_q}})\mathrm{RB_{j_p}}\Phi_{ij}^{n-1/2}\} + \mathrm{RB_{j_N}}\Phi_{ij_N}^{n-1/2} \end{aligned} \tag{91}$$

and the previous time integral

$$\begin{aligned} \Phi_{ij_p}^{n+1/2} = &\mathrm{RE_{j_p}}\Phi_{ij_p}^{n-1/2} - \mathrm{RF_{j_p}}\{(\prod_{q=1}^{p-1} \mathrm{RA_{j_q}})\frac{\partial v_j^{n+1/2}}{\partial j} + \\ &\sum_{m=1}^{p-1} (\prod_{q=m+1}^{p-1} \mathrm{RA_{j_q}})\mathrm{RB_{j_m}}\Phi_{ij_m}^{n-1/2}\} \end{aligned} \tag{92}$$

For all J_{ij}^n and $M_{ij}^{n+1/2}$,

$$\begin{aligned} \mathrm{RA}_{\mathrm{z_p}} &= \frac{2+\Delta t\alpha_{z_p}}{2\kappa_{z_p}+\Delta t(\alpha_{z_p}\kappa_{z_p}+d_{z_p})} \\ \mathrm{RB}_{\mathrm{z_p}} &= \frac{2\kappa_{z_p}}{2\kappa_{z_p}+\Delta t(\alpha_{z_p}\kappa_{z_p}+d_{z_p})} \\ \mathrm{RE}_{\mathrm{z_p}} &= \frac{2\kappa_{z_p}-\Delta t(\alpha_{z_p}\kappa_{z_p}+d_{z_p})}{2\kappa_{z_p}+\Delta t(\alpha_{z_p}\kappa_{z_p}+d_{z_p})} \\ \mathrm{RF}_{\mathrm{z_p}} &= \frac{2d_{z_p}\Delta t}{(2\kappa_{z_p}+\Delta t(\alpha_{z_p}\kappa_{z_p}+d_{z_p}))\kappa_{z_p}} \end{aligned} \tag{93}$$

Outwith the PML region $d = 0, \alpha = 0, \kappa = 1$, resulting in $RA = 1, RB = 1, RE = 1, RF = 0$. This causes J_{ii}, J_{ij}, J_{ik} to reduce to $\partial d_{ij}^{n} / \partial z$ and M_{ii}, M_{ij}, M_{ik} to reduce to $\partial v_j^{n+1/2} / \partial z$. Therefore both stress and velocity equations automatically revert to the original stress derivatives.